HHS Public Access

Author manuscript

Nat Commun. Author manuscript; available in PMC 2016 January 17.

Published in final edited form as:

Nat Commun. ; 6: 7770. doi:10.1038/ncomms8770.

PDGFRβ signaling regulates local inflammation and synergizes with hypercholesterolemia to promote atherosclerosis

Chaoyong He, PhD[1], **Shayna C. Medley**[1,2], **Taishan Hu, PhD**[3], **Myron E. Hinsdale, DVM, PhD**[2,4], **Florea Lupu, PhD**[2,5], **Renu Virmani, MD**[6], and **Lorin E. Olson, PhD**[1,2]

[1]Immunobiology and Cancer Research Program, Oklahoma Medical Research Foundation, 825 NE 13th Street, Oklahoma City, OK 73013, USA

[2]Department of Cell Biology, University of Oklahoma Health Sciences Center, 1100 N Lindsay Ave, Oklahoma City, OK 73104, USA

[3]Fox Chase Cancer Center, 333 Cottman Avenue, Philadelphia, PA 19111, USA

[4]Center for Veterinary Health Sciences, Oklahoma State University, Stillwater, OK, 74074, USA

[5]Cardiovascular Biology Research Program, Oklahoma Medical Research Foundation, 825 NE 13th Street, Oklahoma City, OK 73013

[6]CVPath Institute, Inc., 19 Firstfield Rd, Gaithersburg, MD 20878, USA

Abstract

Platelet-derived growth factor (PDGF) is a mitogen and chemoattractant for vascular smooth muscle cells (VSMCs). However, the direct effects of PDGF receptor β (PDGFRβ) activation on VSMCs have not been studied in the context of atherosclerosis. Here, we present a new mouse model of atherosclerosis with an activating mutation in PDGFRβ. Increased PDGFRβ signaling induces chemokine secretion and leads to leukocyte accumulation in the adventitia and media of the aorta. Furthermore, PDGFRβ^{D849V} amplifies and accelerates atherosclerosis in hypercholesterolemic *ApoE*$^{-/-}$ or *Ldlr*$^{-/-}$ mice. Intriguingly, increased PDGFRβ signaling promotes advanced plaque formation at novel sites in the thoracic aorta and coronary arteries. However, deletion of the PDGFRβ-activated transcription factor STAT1 in VSMCs alleviates inflammation of the arterial wall and reduces plaque burden. These results demonstrate that PDGFRβ pathway activation has a profound effect on vascular disease and support the conclusion that inflammation in the outer arterial layers is a driving process for atherosclerosis.

Correspondence to: Lorin E Olson, PhD, Oklahoma Medical Research Foundation, 825 NE 13th Street, Oklahoma City, OK 73013 Telephone: 405-271-7535, lorin-olson@omrf.org.

Author Contributions

C.H. conducted all experiments except the portions indicated below: S.C.M. performed BrdU labeling, analyzed the data, and edited the manuscript; T.H. assisted with flow cytometry; M.E.H. assisted with electron microscopy; F.L. performed transmission electron microscopy and analyzed the data; R.V. performed Movat's pentachrome stain and analyzed histological samples; C.H. and L.E.O. designed the experiments, analyzed the data, interpreted the data, and wrote the manuscript.

Supplementary Information accompanies this paper including Supplementary Table 1 with primer sequences used for qRT-PCR and five figures.

Competing financial interests: The authors declare no competing financial interests.

INTRODUCTION

Atherosclerosis is a disease of the arteries that remains one of the leading causes of death and disability worldwide. It is characterized by the formation of fatty-fibrous plaques at specific arterial sites through a decades-long process driven by lipoprotein deposition in the vessel wall. This stimulus initiates a cascade of events including leukocyte recruitment and foam cell formation, vascular smooth muscle cell (VSMC) proliferation, changes in extracellular matrix, angiogenesis, calcification, and cell death[1–3]. Most plaques are asymptomatic unless they obstruct blood flow. Other plaques are vulnerable to rupture, which can trigger thrombosis and a deadly risk of sudden heart attack or stroke. However, the interplay of these disease events is not fully understood and is still being explored mechanistically.

Animal models have been invaluable for understanding disease mechanisms in atherosclerosis. The most widely used models are mice with hypercholesterolemia caused by deficiency for apolipoprotein E (*ApoE*$^{-/-}$) or LDL receptor (*Ldlr*$^{-/-}$). These animals develop atherosclerosis over several months compared to decades in humans. However, they do not form the types of advanced plaques that are clinically relevant in humans, nor do they typically develop coronary plaques or experience spontaneous death from heart attack or stroke[4–6]. Therefore, our understanding of advanced plaques is mostly based on descriptive findings from human autopsy studies. To develop a mechanistic understanding of advanced disease processes it is important to generate improved mouse models.

Advanced atherosclerotic plaques develop a morphologically distinct fibrous cap composed of VSMCs that proliferate and migrate from the vessel wall into the plaque[7–9]. Platelet-derived growth factor (PDGF) was first purified over thirty years ago as a serum-derived factor that stimulates VSMC proliferation and migration[10,11]. PDGF is also a potent inducer of VSMC phenotype switching, or dedifferentiation, wherein VSMCs change from a mature, contractile phenotype to a proliferative, secretory phenotype[8,12,13]. PDGF signaling occurs via PDGF receptors (PDGFRs), which are prototypical of receptor tyrosine kinases. In the absence of PDGF ligand, PDGFR tyrosine kinase activity is inhibited by an autoinhibitory allosteric conformation; ligand binding alters the conformation to allow physiological signaling activity. PDGF signaling via PDGFRβ has been associated with vascular disease and is suspected to play a major role in VSMC migration and proliferation during atherosclerosis[14,15]. In *ApoE*$^{-/-}$ mice, blockade of the PDGF-PDGFRβ pathway with neutralizing antibodies or chemical inhibitors reduced VSMC involvement in atherosclerosis[16,17]. It seems likely that increased PDGF signaling would stimulate more VSMC involvement in atherosclerosis and potentially drive the formation of more aggressive atherosclerosis in mice. This approach has not been explored previously.

Here, we take advantage of knockin mice having a Cre-inducible D849V point mutation in the endogenous PDGF receptor β gene (*PDGFRβ*^{D849V})[18], which we activate with a Sm22α-Cre driver to initiate signaling in VSMCs. The D849V mutation destabilizes the autoinhibited conformation of the receptor and thereby increases basal and ligand-mediated PDGFRβ signaling. We show that PDGF signaling increases chemokine signaling from VSMCs and causes inflammation of the aorta, in addition to causing VSMC phenotype

switching and architectural changes in the muscle layer of the aorta. Using this model we test the hypothesis that PDGF-driven changes in VSMC phenotype and function synergize with hypercholesterolemia to promote the formation of advanced atherosclerotic plaques. Surprisingly, increased PDGF signaling not only promotes the formation of advanced plaque morphologies but it also enhances the initiation of new plaques at a plaque-resistant site, the thoracic aorta. Cells respond to PDGF signaling by phosphorylating transcription factors of the signal transducer and activator of transcription (STAT) family, and STAT1 in particular is known to regulate chemokine gene expression. Experiments with the kinase inhibitor Ruxolitinib suggest that PDGFRβ phosphorylation of STAT1 requires the activity of JAK1/2 tyrosine kinases. By deletion of a STAT1-floxed allele in VSMCs, we show that PDGF-driven chemokine signaling and inflammation are STAT1-dependent. Finally, in the context of PDGF-driven atherosclerosis, deletion of STAT1 from VSMCs reduces plaque formation, demonstrating that inflammation of the arterial media and adventitia are important mechanisms by which PDGF signaling promotes atherosclerosis.

RESULTS

PDGF signaling induces chemokine production from VSMCs

We previously showed that a Cre-inducible gain-of-function knockin mutation in PDGFRβ (PDGFRβ^{D849V}) induced chemokine mRNA expression in brain pericytes and caused inflammation of the central nervous system[18]. To characterize chemokine expression specifically in VSMCs of the aorta, which was not previously tested, we generated *Sm22α-Cre;PDGFRβ*$^{+/D849V}$ (*PDGFRβ*^{Sm22D849V}) conditional mutant mice and *Sm22α-Cre;PDGFRβ*$^{+/+}$ littermate controls (designated as Wt) (Fig. 1a). We then established primary VSMC cultures from mutant and control aortas and examined the expression of chemokines that we previously identified by microarray. Using quantitative RT-PCR (qRT-PCR) we found upregulated mRNA levels for chemokines known to regulate monocyte (CCL2, CCL3, CCL5, CCL6, CCL7, CCL9, CCL12) and T cell recruitment (CXCL9, CXCL10, CXCL11) (Fig. 1b). We also detected increased chemokine secretion in conditioned media from mutant VSMCs (Fig. 1c). Mouse plasma contains much lower levels of chemokines compared to conditioned media, but even with this limitation we detected increased levels of circulating CCL2 and CCL3 in the plasma of *PDGFRβ*^{Sm22D849V} mice (Fig. 1d). Chemokine expression could be induced by treating control VSMCs with PDGF-BB (Fig. 1e). However, other known inflammatory signals, namely IL-1β, TNF-α, IFN-α, IFN-β and IFN-γ, were not upregulated in mutant VSMCs compared to controls (by qRT-PCR, data not shown). Thus, PDGFRβ signaling in VMSCs induces several chemokines, many of which are known to be involved in atherosclerosis[19].

PDGF signaling in VSMCs causes inflammation of the aorta

Based on our finding of increased chemokine secretion by *PDGFRβ*^{Sm22D849V} VSMCs, we sought to assess the resident leukocyte populations in the wall of the aorta. By flow cytometric analysis of enzymatically digested control and mutant thoracic aortas, we found that mutants carried a 7-fold increase in the total number of CD45^{+} leukocytes (Fig. 2a, b and Supplementary Figure 1). The majority of the leukocytes were found in the adventitia, which is a normal site for small populations of leukocytes to reside in a non-atherosclerotic

aorta (Fig. 2c)[20–22]. Histological analysis also provided evidence of abundant accumulated leukocytes in the mutant aorta adventitia and media (Fig. 2d). Further flow-cytometric analysis revealed increased numbers of leukocytes expressing CD3, CD19, CD11b, CD11c, and NK1.1 in the mutant aortas (Fig. 2e). These data suggest that PDGF signaling in VSMCs induces signals, likely to be chemokines, which create an inflammatory milieu in the wall of the thoracic aorta. To investigate whether short-term pharmacological inhibition of PDGFRβ could reduce inflammation in the vessel wall, we treated *PDGFRβ*^{Sm22D849V} mice with Crenolanib, a tyrosine kinase inhibitor specific for class III receptors. After 5 days of treatment, we found a decrease in the number of leukocytes in mutants that received the drug compared to untreated mutants (Fig. 2f, g). This suggests that continual PDGFRβ activation sustains inflammation.

Constitutive dedifferentiation of VSMCs

As suggested previously[18], *PDGFRβ*^{Sm22D849V} mutant mice have constitutively dedifferentiated VSMCs and exhibit VSMC hyperplasia (Fig. 3a), decreased expression of contractile proteins SMMHC, SM22α, and αSMA (Fig. 3B), and increased extracellular matrix (ECM) production (Fig. 3c, d). Further analysis showed a cellular ultrastructure consistent with a phenotypic switch, where instead of contractile bundles there was an abundance of rough endoplasmic reticulum in mutant VMSCs (Fig. 3e). Due to VSMC hyperplasia and stiffening of the vessel wall, the thoracic aorta in *PDGFRβ*^{Sm22D849V} mutants undergoes adaptive remodeling to become approximately 2-fold larger in diameter by 4 weeks of age, as shown previously[18]. We found no significant difference in blood pressure between adult mutants and controls (mutant: systolic 96.6±2.8/diastolic 73.3±5.8 mmHg; control: systolic 108.3±8.3/diastolic 77.6±4.2 mmHg; mean ± s.e.m., n=6 mice per genotype).

PDGF signaling amplifies atherosclerosis

Inflammation, VSMC dedifferentiation, and aortic enlargement in PDGFRβ^{Sm22D849V} mice provided clues that they might be more susceptible to atherosclerosis than normal mice. In particular, vascular inflammation is an early event in atherosclerosis, and VSMC dedifferentiation is characteristic of later disease. However, the most important risk factor for atherosclerosis is high cholesterol and *PDGFRβ*^{Sm22D849V} mice had normal cholesterol and triglyceride levels compared to control counterparts (Table I). Accordingly, we did not detect atherosclerotic plaques up to 1 year of age whether the mutants were fed a normal chow or Western diet (WD). Therefore, to produce hypercholesterolemia we backcrossed *PDGFRβ*^{Sm22D849V} mice onto an *ApoE*-deficient genetic background to generate *ApoE*$^{-/-}$*;Sm22α-Cre;PDGFRβ*$^{+/D849V}$ (*ApoE,PDGFRβ*^{Sm22D849V}) mutant mice and *ApoE*$^{-/-}$*;Sm22α-Cre;PDGFRβ*$^{+/+}$ (*ApoE*) littermate controls. Thus, serum lipid profiles increased as expected (Table I).

After 16 weeks of WD we assessed atherosclerotic plaque formation by two common methods: Oil red O staining for plaques on the luminal surface of flat-mounted aortas, and cross sectional analysis of plaques in the aortic root. Both approaches revealed a dramatic increase in plaque formation in *ApoE,PDGFRβ*^{Sm22D849V} mice. Flat-mounted *ApoE* aortas exhibited plaques in the aortic arch, the brachiocephalic artery (BCA), and occasionally at

branch points to the renal arteries, which are typical sites of plaque formation. In contrast, *ApoE,PDGFRβ*^{Sm22D849V} aortas exhibited confluent plaques throughout the aortic tree, including the typically plaque-resistant thoracic aorta (Fig. 4a). Similarly, plaques in the aortic root were larger in the *ApoE,PDGFRβ*^{Sm22D849V} mice and they exhibited an advanced morphology with well-defined fibrous caps overlying acellular necrotic cores (Fig. 4b). Necrotic core area was much larger and fibrous cap thickness was reduced in *ApoE,PDGFRβ*^{Sm22D849V} aortic root plaques compared to *ApoE* (Supplementary Figure 2b, c). *ApoE,PDGFRβ*^{Sm22D849V} aortic root plaques were enriched for macrophages as a percent of plaque area (Supplementary Figure 2a). Gene expression analysis suggested that macrophages in *ApoE,PDGFRβ*^{Sm22D849V} plaques were more of the M1 (pro-inflammatory) phenotype than M2, in comparison to *ApoE* (Supplementary Figure 3).

To carefully track plaque progression over time we quantified cross-sectional plaque area after 6, 8, 16, and 24 weeks of WD, measuring plaques in the aortic root, aortic arch, BCA, and thoracic aorta (Fig. 4c). At all time points and all sites examined, plaques were significantly larger in *ApoE,PDGFRβ*^{Sm22D849V} aortas. We also performed quantification of cross-sectional plaque area in a cohort of mice with chow diet feeding, where moderate hypercholesterolemia results in slower plaque development. We examined time points between 6 and 12 months of age, and found that *ApoE,PDGFRβ*^{Sm22D849V} aortas still developed distinctive plaques in the thoracic aorta and larger plaques at other sites compared to *ApoE* controls (Fig. 4d).

We wanted to ensure that the synergistic effect of PDGF signaling and hypercholesterolemia was not specific to the *ApoE* mutant. Therefore, we crossed *PDGFRβ*^{Sm22D849V} mice with mice deficient for low-density lipoprotein receptor (LDLR), which also causes hypercholesterolemia. We compared *Ldlr* and *Ldlr,PDGFRβ*^{Sm22D849V} mutants after 16 weeks of WD feeding and again found a striking increase in atherosclerotic plaque area in *Ldlr,PDGFRβ*^{Sm22D849V} aortas (Fig. 4e, f). This finding is important because ApoE itself can influence PDGFRβ activity by interacting with LDL receptor-related protein-1 (LRP1) to attenuate PDGFRβ function[23,24]. The finding that PDGFRβ^{D849V} synergizes with *Ldlr* argues that the effects shown here are not attributable to lack of inhibition from the ApoE-LRP1 complex. Taken together, the results from ApoE/WD, ApoE/chow, and Ldlr/WD studies clearly demonstrate that increased PDGF signaling in VSMCs strongly amplifies atherosclerosis under a variety of hypercholesterolemic conditions.

Plaque progression to fibroatheroma and hemorrhage

We performed careful morphological assessment of the thoracic aorta plaques in *ApoE,PDGFRβ*^{Sm22D849V} mice because of their striking size and unusual location. At 6 weeks of WD the plaques initiated as accumulations of foam cell macrophages within the intima (Fig. 5a, Supplementary Figure 4). By 8 weeks of WD, smooth muscle cells were seen invading the foam cell-rich plaques and fibrous cap structures began to form at this time (Fig. 5b, black arrows). By 16 and 24 weeks of WD, the plaques had reached a fibrous cap atheroma stage[4], exhibiting well-formed collagen-rich fibrous caps and large necrotic cores (Fig. 5c, d, e). An additional feature seen at 16 weeks WD and later was areas of hemorrhage within advanced fibroatheroma plaques (seen in 7 of 10 mutants, Fig. 5f).

Cross-sectioning through such areas showed that hemorrhages were contained within the plaque without evidence of a ruptured fibrous cap (Fig. 5g). Iron deposition at hemorrhage sites was evident by Prussian blue stain (Fig. 5h). In advanced human atherosclerosis, neovascularization of plaques is associated with increased inflammation, intraplaque hemorrhage, and increasing plaque vulnerability[25,26]. Accordingly, we observed $PECAM^{+}$ microvessels in advanced plaques of *ApoE,PDGFRβ*^{Sm22D849V} mice (Fig. 5i). Together, these data demonstrate that *ApoE,PDGFRβ*^{Sm22D849V} mice readily develop plaques with advanced morphologies much like those seen in humans. Fibroatheromas with these features are extremely rare (or nonexistent) in standard *ApoE* and *Ldlr*-deficient mouse models.

Coronary atherosclerosis

Coronary artery plaques are not typical in *ApoE* single mutant mice unless they are fed a WD for 10 months[27,28]. We observed coronary atherosclerosis in some of the *PDGFRβ*^{D849V} cohorts. This was observed in 70% (7 of 10) *ApoE,PDGFRβ*^{Sm22D849V} mice that were fed a chow diet for 10–12 months (Fig. 6a, b) and in 71% (5 of 7) *Ldlr,PDGFRβ*^{Sm22D849V} mice that were fed WD for 16 weeks (Fig. 6c, d). Some of these plaques appeared to be fibroatheromas (Fig. 6b). Sudden deaths occurred in some *ApoE,PDGFRβ*^{Sm22D849V} mice as early as 12 weeks of WD, and 50% died by 19 weeks of WD (n = 26) (Supplementary Figure 5). It is possible that coronary plaques contributed to the reduced viability of WD-fed mutants, but this needs to be investigated further in a study specifically designed to identify causes of death.

PDGF signaling activates STAT1 in VSMCs

The striking amplification of atherosclerosis raised mechanistic questions about which PDGF-regulated processes actually drive the atherosclerotic phenotype and which processes are bystanders. Clearly, inflammation is seen throughout atherogenesis. On the other hand, VSMC hyperplasia, phenotype switching, and increased ECM synthesis seemed important for helping early plaques to progress to the fibroatheroma morphology. Therefore, we hypothesized that PDGF-induced chemokine secretion and inflammation of the vessel wall (see Fig. 1 and Fig. 2) were the processes driving plaque initiation. PDGFRβ regulates several downstream signaling cascades including Ras/MAP kinase, PI3 kinase/AKT, PLCγ/PKC, and STATs. We chose to focus on STAT1 as a potential mediator of pro-inflammatory PDGFRβ signaling because this transcription factor is a direct activator chemokine gene expression in the context of interferon signaling[29].

First, *PDGFRβ*$^{+/+}$ (Wt) control VSMCs were incubated with or without interferon gamma (IFN-γ) and STAT1 phosphorylation was assessed. IFN-γ was required for STAT1 phosphorylation in control VSMCs, but STAT1 was constitutively phosphorylated in *PDGFRβ*^{Sm22D849V} cells (Fig. 7a). This was specific to STAT1, as STAT3 and STAT5 were not phosphorylated in mutant cells. Treatment of control VSMCs with PDGF resulted in STAT1 phosphorylation (Fig. 7b), and treatment of *PDGFRβ*^{Sm22D849V} cells with the PDGFR inhibitor AG-1295 abolished STAT1 phosphorylation (Fig. 7c, d), indicating that constitutive STAT1 phosphorylation depends on PDGF pathway activity. AG-1295 had no effect on STAT1 phosphorylation in response to IFN-γ treatment (Fig. 7e, f, fourth lane), indicating that PDGFRβ is not required for this response. The constitutively phosphorylated

STAT1 in *PDGFRβ*^{Sm22D849V} VSMCs could be further phosphorylated by the addition of exogenous IFN-γ (Fig. 7e, f, seventh lane), suggesting that *PDGFRβ*^{Sm22D849V} VSMCs remain capable of sensing interferon. However, as discussed previously, we did not detect increased interferon (IFN-α, β, or γ) mRNA expression in *PDGFRβ*^{Sm22D849V} VSMCs compared to control cells, consistent with the model that PDGFRβ signaling is responsible for the phosphorylation of STAT1.

In the IFN-γ signaling cascade, activated interferon receptors recruit Janus-activated kinase (JAK)-1 and -2, which are cytoplasmic tyrosine kinases that subsequently phosphorylate STAT1. Previous studies found that PDGFRβ associates with and phosphorylates JAK1, JAK2, and the related kinase Tyk2, but suggested that, unlike the interferon pathway, JAKs may be dispensable for PDGFRβ-induced STAT1 activation[30,31]. To explore this question in VSMCs we treated control or mutant cells and the JAK1/2-selective inhibitor Ruxolitinib (Rux). As expected, pretreatment of VSMCs with Rux blocked STAT1 phosphorylation in response to IFN-γ (Fig. 7g, h, fourth lane). Interestingly, Rux also blocked STAT1 phosphorylation in control VSMCs treated with PDGF-BB, and in unstimulated *PDGFRβ*^{Sm22D849V} VSMCs (Fig. 7g, h, sixth and eighth lanes). This points to the conclusion that JAK1 and/or JAK2 are required for STAT1 phosphorylation in the PDGF signaling pathway. As a control, Rux had no effect on PDGFRβ-induced PLCγ1 phosphorylation, indicating that Rux does not impair PDGFRβ tyrosine kinase activity.

STAT1 regulates chemokine production and inflammation

We tested whether STAT1 could regulate chemokine expression using siRNA knockdown and genetic approaches. Transfection of *PDGFRβ*^{Sm22D849V} VSMCs with STAT1-siRNA significantly reduced total and phospho-STAT1 protein levels (Fig. 8a). qRT-PCR of *PDGFRβ*^{Sm22D849V} VSMCs transfected with STAT1-siRNA showed reduced mRNA expression for seven out of ten chemokines compared to control siRNA (Fig. 8b). Next, we obtained *STAT1*$^{flox/flox}$ mice[32] and bred them with *PDGFRβ*^{Sm22D849V} mutants. Deletion of STAT1 protein from VSMCs was confirmed by Western blot (Fig. 8c). We then compared chemokine expression in VSMCs from Wt, *STAT1*^{Sm22CKO} (STAT1-cKO) single mutant, *PDGFRβ*^{Sm22D849V} (β-D849V) single mutant, and *STAT1*^{Sm22CKO}*PDGFRβ*^{Sm22D849V} (β-D849V,STAT1-cKO) double mutant mice. In agreement with the siRNA knockdown, *STAT1*^{Sm22cKO}*PDGFRβ*^{Sm22D849V} cells had significantly reduced expression of CCL2, CCL5, CCL7, CCL12, CXCL9, CXCL10, and CXCL11 compared to *PDGFRβ*^{Sm22D849V} cells (Fig. 8d). Therefore, the PDGF signaling pathway regulates chemokine expression by a STAT1-dependent mechanism. We further investigated if STAT1 deletion could modify PDGFRβ-driven leukocyte accumulation in the aortic wall. We performed flow cytometry on thoracic aortas (*ApoE*$^{+/+}$) and found that CD45^{+} leukocyte accumulation was reduced to almost wild-type levels in *STAT1*^{Sm22cKO}*PDGFRβ*^{Sm22D849V} aortas (Fig. 8e, compare to Fig. 2b). Interestingly, while STAT1 deletion prevented inflammation, downregulation of VSMC differentiation markers still occurred (Fig. 8f, compare to Fig. 3b) and aortic dilation was still observed. Thus, STAT1 regulates VSMC chemokine production and aortic inflammation downstream of PDGFRβ but it is not required for VSMC dedifferentiation.

PDGF/STAT1-regulated inflammation amplifies atherosclerosis

PDGFRβ^{Sm22D849V} aortas exhibit inflammation and dedifferentiated VSMCs, and deletion of STAT1 in VSMCs reduces inflammation but does not affect the VSMC phenotype (Fig. 8). This suggested that STAT1 deletion in *ApoE,PDGFRβ*^{Sm22D849V} mice would be an approach to evaluate the importance of inflammation vs. VSMC dedifferentiation as pro-atherosclerotic mechanisms. To test this we generated *ApoE,PDGFRβ*^{Sm22D849V} single conditional mutants with hypercholesterolemia and *ApoE*$^{-/-}$*;STAT1*$^{flox/flox}$*;Sm22α-Cre;PDGFRβ*$^{+/D849V}$ (*ApoE,STAT1*^{Sm22cKO}*PDGFRβ*^{Sm22D849V}) double conditional mutants with hypercholesterolemia. After feeding WD for 12 weeks we screened for atherosclerosis. Compared to *ApoE,PDGFRβ*^{Sm22D849V} mutants, a much smaller area of the aorta was covered by plaques in *ApoE,STAT1*^{Sm22cKO}*PDGFRβ*^{Sm22D849V} mutants that were lacking STAT1 in VSMCs (Fig. 9a, b). Moreover, plaques in the aortic root of the double mutants were significantly smaller than those of the single mutants (Fig. 9c, d), appearing similar to the size of plaques in *ApoE*$^{-/-}$ aortic roots at 8–16 weeks of WD (Fig. 4c). Next, we examined plaque composition in the thoracic aorta. After 12 weeks of WD the less abundant plaques in *ApoE,STAT1*^{Sm22cKO}*PDGFRβ*^{Sm22D849V} mutants were clearly less advanced with poorly developed fibrous caps and small necrotic cores compared to *ApoE,PDGFRβ*^{Sm22D849V} mutants (Fig. 9e). Therefore, PDGFRβ-STAT1 signaling in VMSCs creates an inflammatory milieu in the aortic adventitia and media that strongly predisposes arteries to form atherosclerotic plaques in synergy with hypercholesterolemia.

DISCUSSION

The mechanisms that control the initiation and progression of atherosclerosis are incompletely understood. In this study, we investigated the effects of increased PDGFRβ signaling on atherosclerosis. We first showed that conditional activation of PDGFRβ induced the expression of chemokines in VSMCs and caused inflammation of the aortic media and adventitia in *PDGFRβ*^{Sm22D849V} mutant mice. Taken together with VSMC dedifferentiation, hyperplasia, and increased ECM synthesis, these phenotypes suggested that the activating mutation in PDGFRβ would be pro-atherogenic. Analysis of *ApoE,PDGFRβ*^{Sm22D849V} mice provided clear evidence that PDGF signaling strongly amplified hypercholesterolemia-induced atherosclerosis. Intriguingly, increased PDGF signaling expanded the sites of plaque initiation, allowing atherosclerosis to occur in the thoracic aorta and coronary arteries that are typically free of plaques in *ApoE* or *Ldlr* single mutant mice. In *ApoE,PDGFRβ*^{Sm22D849V} mice, the plaques consistently developed into fibroatheromas. Moreover, the aortic plaques exhibited neovascularization and intraplaque hemorrhage, which are common in advanced atherosclerotic lesions in humans. Neovascularization is thought to contribute to disease by providing a route for macrophages and other leukocytes to enter the plaques[33]. Intraplaque hemorrhage worsens atherosclerosis by depositing large amounts of free cholesterol from erythrocyte membranes[25,26]. In addition, iron deposits in atheromas may worsen atherosclerosis by increasing the formation of reactive oxygen species and oxidized LDL[34]. *ApoE*$^{-/-}$ mice do not typically develop coronary atherosclerosis without long-term (10 months) of WD feeding[27,28]. *ApoE*$^{-/-}$*Akt1*$^{-/-}$ double mutants develop coronary atherosclerosis after 14 weeks of high cholesterol diet through mechanisms involving increased endothelial cell and macrophage

apoptosis[35]. More dramatically, scavenger receptor B1 (SR-BI)-deficient mice on an *ApoE*$^{-/-}$ background develop severe coronary atherosclerosis by 5 weeks of age due to profound alterations in lipoprotein metabolism[36]. Thus, the *PDGFRβ*^{Sm22D849V} mice combined with *ApoE* or *Ldlr* mutations provide a distinct model of atherosclerosis that may help define the role of VSMCs in plaque advancement and coronary heart disease.

We provided genetic evidence that inflammation directly contributes to novel plaque formation in the thoracic aorta. Conditional deletion of STAT1 in *ApoE*$^{+/+}$ VSMCs was sufficient to normalize much of the chemokine overexpression and inflammation caused by PDGF signaling. However, VSMC phenotype switching and adaptive remodeling (dilation) of the aorta persisted in *STAT1*^{Sm22cKO}*PDGFRβ*^{Sm22D849V} double-mutant mice, indicating that these aspects of the phenotype are not dependent on STAT1. Even though aortic dilation persisted in double mutants, far fewer plaques occurred in the thoracic aorta. Thus, our data point to an inflammatory pathway as an important mechanism by which PDGF signaling amplifies atherosclerosis. We cannot completely exclude possible hemodynamic changes secondary to remodeling of the aorta as a contributing factor towards enhanced atherosclerosis, but our genetic evidence demonstrates that STAT1-linked inflammation is required. This inflammatory pathway involves PDGFRβ activation in VSMCs, activation of JAKs, tyrosine phosphorylation of STAT1, secretion of chemokines from VSMCs, and accumulation of leukocytes in the adventitia and media of the aortic wall. Leukocyte accumulations were apparent in histological sections of *PDGFRβ*^{Sm22D849V} adventitia (Fig. 2d). Intriguingly, recent studies highlight the potential of VSMCs to act as lymphoid tissue organizers by secreting chemokines (CXCL13, CCL21, and others) that promote lymphoid tissue neogenesis[37,38]. Furthermore, aged *ApoE*$^{-/-}$ mice develop tertiary lymphoid tissue in the aorta adventitia[39]. As we did not find well-organized lymphoid tissue in the adventitia, the relevance of these observations to our model is unknown. It is possible that our mice were too young at the time of analysis, or that the chemokines involved are not sufficient for the formation of organized lymphoid tissue. Specific chemokines we identified as STAT1-dependent PDGF targets have been previously shown to have pro-atherogenic functions. CCL2/MCP-1 and CCL5/RANTES are important chemoattractants for monocytes and macrophages in the atherosclerotic setting[40–43]. CXCL10/IP-10 modulates the balance of effector and regulatory T cells in atherosclerosis by activating the receptor CXCR3[44,45]. There is evidence to suggest that the related chemokines CXCL9/MIG and CXCL11/ITAC also regulate T cell trafficking in atherosclerosis[45–47]. Together, these data suggest that chemokines released by VSMCs work together to inflame the aorta, which may create new niches for plaque initiation when combined with hypercholesterolemia.

Arterial VSMCs have long been viewed as one of the major cell types involved in atherosclerosis[48]. Most recent work on plaque initiation has focused on the importance of inflammatory cells and endothelial cells, while VSMCs are more often discussed in the context of advanced atherosclerosis when VSMCs switch from a contractile to a secretory phenotype, proliferate, migrate into plaques, and create fibrous cap structures. However, from human autopsy studies it is known that VSMCs predominate in the thickened arterial intima at atherosclerosis-prone sites even prior to the onset of plaque formation[49–51]. Therefore, it has been suggested that VSMCs might help initiate plaques at atherosclerosis-

prone sites by transdifferentiating into foam cells[52,53], by producing proteoglycans that trap lipoproteins[54], by expressing adhesion molecules that recruit inflammatory cells[55], or by enhancing the activity or survival of monocytes and macrophages[56]. Further investigation may reveal whether any of these disease processes are exacerbated in *PDGFRβ*^{Sm22D849V} mice and whether they are modulated by the loss of STAT1.

The D849V mutation in PDGFRβ increases basal and ligand-mediated signaling activity of PDGFRβ, which leads to constitutive phosphorylation of STAT1 in a JAK1/2-dependent manner. Phosphorylation of STAT1 in PDGF-treated cells was demonstrated over 20 years ago[57], and our study now shows an *in vivo* role for the PDGFRβ-STAT1 signaling pathway in regulating the VSMC inflammatory phenotype. STAT1 knockout mice do not exhibit vascular phenotypes under basal conditions[58,59]. However, STAT1 may operate in VSMCs in a context-dependent manner, for instance during the response to injury and inflammation. STAT1 may be especially important under conditions where IFN-γ and PDGF are both present, as previous studies suggested interactions between the two signaling pathways[60–63]. Further work will be needed to understand the importance of VSMC-expressed STAT1 for atherosclerosis in standard *ApoE* and *Ldlr*-deficient mice.

This study shows that increased PDGFRβ signaling causes inflammation and VSMC dedifferentiation *in vivo*. In the setting of hypercholesterolemia, PDGFRβ signaling promotes new plaque initiation at atherosclerosis-resistant sites and promotes the formation of fibroatheroma plaques with neovascularization and plaque rupture. A novel aspect of this study is the observation that initiation of plaques in the subendothelium of thoracic aorta requires inflammation of the adventitia and media. The conventional model of atherosclerosis has focused on the inner layers of the vessel, guided by the paradigm of endothelial cell activation, subendothelial inflammation, monocyte recruitment to the subendothelium, and foam cell formation in the subendothelium. This view emphasizes inflammation beginning at the luminal side of the vessel wall and progressing outward, with the outer layers of the vessel playing a passive role. However, the present study contributes experimental evidence pointing towards the importance of outside-in mechanisms where inflammation of the adventitia and media creates new niches for atherosclerotic plaque initiation.

METHODS

Mice

Sm22α-Cre;PDGFRβ$^{+/D849V}$ (*PDGFRβ*^{Sm22D849V}) conditional knockin mice[18] were crossed to *ApoE* or *Ldlr*-deficient mice obtained from the Jackson Laboratory. *STAT1*$^{flox/flox}$ mice were provided by L. Hennighausen (NIDDK, NIH, Bethesda, MD)[32]. Collagen1a1-EGFP transgenic reporter mice were provided by D. Brenner (UCSD, La Jolla, CA)[64]. All mice were maintained on a mixed C57BL/6;129 background and were fed standard chow or Western diet (diet#TD88137, Harlan Teklad). Some mice were injected with 15mg kg^{-1} Crenolanib (Selleck Chemicals) for 5 consecutive days. Mutant mice were always compared to age and sex-matched controls that carried the appropriate Cre driver, and littermates were used whenever possible. We did not observe any vessel aneurism development (defined as focal dilation/weakening of the vessel wall), aortic dissection, kidney failure, or tumor

formation in any of the *PDGFRβ*^{Sm22D849V} mutants we examined during the period of our study. All animal experiments were performed under approval from the Institutional Animal Care and Use Committee of the Oklahoma Medical Research Foundation.

Isolation and culture of primary VSMCs

Mouse VSMCs were isolated by the explant method from aortas of 6–8 weeks old mice[65]. VSMCs were cultured in DMEM medium plus 10% FBS and antibiotics. All assays were performed at passages 2 to 5. To induce chemokine expression, wild type VSMCs were serum starved in DMEM + 0.5% FBS for 36 hrs, followed by stimulation with 10ng ml^{-1} PDGF-BB (R&D Systems). For STAT phosphorylation experiments, 10ng ml^{-1} mouse IFN-γ (EMD Millipore) served as a positive control. To block PDGFRβ activity, VSMCs were treated with 400ng ml^{-1} Crenolanib (Selleck Chemicals) for 2 hrs or 10 μM AG-1295 (Calbiochem) for 16 hrs. To block JAK1/JAK2 kinase activity, VSMCs were treated with 10 μM Ruxolitinib (Selleck Chemicals) for 16 hrs. STAT1 siRNA and nonsilencing control siRNA were obtained from Santa Cruz Biotechnology. Mouse VSMCs were transfected with siRNA for 48 hrs using Lipofectamine RNAiMAX (Invitrogen) according to the manufacturer's instructions.

RNA isolation and quantitative RT-PCR

Total RNA was extracted from cultured VSMCs using RNeasy Mini Kit (Qiagen). Reverse transcription to cDNA was performed using random primers and Superscript III RT (Invitrogen). Quantitative real-time PCR was performed using a Bio-Rad iCycler with iQ TM SYBR green master mix. Results were normalized relative to GAPDH unless indicated otherwise.

Quantification of mouse chemokine proteins

Mouse VSMCs were cultured in 6-well plates. Chemokine protein levels in harvested conditioned media and mouse plasmas were determined using a multi-analyte ELISA kit (Qiagen MEM-009A) according to the manufacturer's instructions.

Aorta flow cytometry analysis

Single-cell suspensions were prepared from the mouse aortas as described[20]. Briefly, mice were anesthetized and perfused through the heart with PBS containing 10 U ml^{-1} heparin to remove blood from all vessels. After careful removal of the perivascular adipose tissue, the aortas were minced into small pieces and digested with 125 U ml^{-1} collagenase type XI, 60 U ml^{-1} hyaluronidase type I-s, 60 U ml^{-1} DNase1, and 450 U ml^{-1} collagenase type I (all enzymes were obtained from Sigma-Aldrich) in PBS containing 20 mM Hepes at 37°C for 3 hrs. For separating adventitia and media, the aortas were predigested in enzyme cocktail (300U ml^{-1} Collagenase I and 10U ml^{-1} Elastase in PBS) at 37°C for 15 minutes and then the adventitia was carefully peeled away from the aorta. After filtering through a 70 μm filter, cells were resuspended in FACS buffer, and incubated with Fc-blocking antibody (eBioscience) for 15 min on ice before being stained with specific antibodies. Antibodies used were as follows: FITC-CD45.2, PE-CD11c, APC-CD3, APC-Cy7-CD19, PE-Cy7-NK1.1, PerCy5.5-CD11b (all antibodies were obtained from Biolegend and used at 1:100

dilution). Cells were also stained with propidium iodide. After washing, immunofluorescence was detected by an LSR II (BD Biosciences). Data were analyzed using FlowJo (Tree Star Inc.) software.

Immunoprecipitation and Western blotting

VSMCs were lysed in RIPA buffer and protein contents were measured using the BCA assay. Total lysates were immunoprecipitated with antibody against PDGFRβ (Santa Cruz Biotechnology, sc-432). Immunoprecipitates or cell lysates were subjected to Western blotting with antibodies to phospho-STAT1 (Invitrogen 333400), phospho-STAT3 (Cell Signaling, 9145), phospho-STAT5 (Cell Signaling, 9359), β-Actin (Cell Signaling, 4970L), phospho-Tyrosine (Millipore, 05–321), total STAT1 (Millipore, 06–501), total PLCγ1 (Cell Signaling 2822), and phosphor-PLCγ1 (Cell Signaling 14008). Primary antibodies were used at 1:1000. HRP-conjugated secondary antibodies (Jackson ImmunoResearch) were used at 1:5000.

BrdU incorporation and labeling index

Mice were injected with 50mg kg^{-1} BrdU and then sacrificed 24 hrs later. Aortas were perfused with PBS/heparin, perfusion fixed with 4% paraformaldehyde (PFA), paraffin embedded, and sectioned longitudinally. Cells were identified as VSMCs based on their position between the internal and external elastic lamina of the tunica media. Proliferating VSMCs ($BrdU^{+}$) were detected with anti-BrdU antibody (Sigma) at 1:20 dilution. Hematoxylin was used as a counterstain for nuclei.

Blood pressure measurements

Blood pressure was measured by the carotid catheter method. 8–10 weeks old mice were anesthetized with a ketamine and xylazine mixture (70:6 mg kg^{-1}, intramuscular injection) and placed under warm light (37°C). The left common carotid artery was carefully exposed via a 0.5- to 1.0-cm midline incision in the ventral neck region. The tip of the artery toward the head was ligated with a suture (5–0 silk), and the tip toward heart was occluded with a microclip (no. 18055–03; Fine Science Tool, Foster City, CA). A small cut was then made in the vessel wall using microscissors (no. 15000–08, Fine Science Tool). A catheter (PE10 tubing) containing a sterile 10% heparin-90% saline solution was inserted into the common carotid. Blood was directed to a pressure transducer through the catheter to obtain computerized blood pressure measurements (AD instruments) after removing the clip. (mean ± s.e.m. n = 6 mice per group).

Serum lipid profiles

Wild type or *PDGFRβ*^{Sm22D849V} mice from both sexes were fed chow diet for 2–3 months or WD for 24 weeks. *ApoE* and *ApoE,PDGFRβ*^{Sm22D849V} mice were fed chow diet for 8–10 months or WD for 16 weeks. Blood was drawn from the facial vein with light anesthesia and serum was separated by centrifugation. Cholesterol and triglyceride levels were determined by commercially available kits (BioVision and ThermoScientific) followed by spectrophotometric quantification.

Qualitative analysis of tissues and atherosclerotic plaques

For immunohistochemistry, perfused aortas were post-fixed in 4% PFA overnight, then cryosectioned at 8 μm and stained with primary antibodies recognizing PECAM (BD Bioscience 553370, 1:100), αSMA (Sigma F3777, 1:250), MOMA-2 (AbD Serotec MCA519G, 1:100), F4/80 (Abcam ab6640, 1:100), SMMHC (Biomedical Technologies Inc. BT-562, 1:100) or Sm22α (Abcam ab10135, 1:100), with appropriate donkey secondary antibodies (Jackson ImmunoResearch). Immunofluorescence microscopy was performed with a Nikon Eclipse 80*i* microscope connected to a digital camera. Final image processing was performed with Photoshop (Adobe). For histological stains, perfused aortas were post-fixed with Bouin's solution, paraffin embedded, and sectioned at 5 μm before staining with Movat's pentachrome, Masson's trichrome, or Prussian blue. Formalin-fixed aortic roots were cryosectioned at 10 μm and stained with Oil red O.

Quantitative analysis of plaques

Mice were perfused by cardiac puncture with PBS containing 10U ml^{-1} of heparin and then 4% PFA, followed by overnight post-fix with 10% formalin. For *en face* staining, the adventitia was thoroughly cleaned under dissecting microscope, and the aorta was cut open longitudinally and pinned on parafilm. Plaques were stained with Oil red O and photographed with a digital camera. For cross-sectional quantification of plaque progression, 5μm serial paraffin sections from the indicated sites of the aorta were stained with hematoxylin and eosin. Plaques were imaged with a Nikon Eclipse 80*i* microscope connected to a digital camera. Plaque area was then quantified with NIS.Elements D3.2 imaging software (Nikon Inc.) to obtain the maximum cross-sectional plaque area for each site. Fibrous cap thickness was quantified by choosing the largest necrotic core in a section and measuring the thinnest part of the fibrous cap. Representative images were finally processed with Photoshop (Adobe).

Transmission Electron Microscopy

Two week-old mice were perfusion fixed through the heart, then thoracic aorta segments were isolated and immersion fixed with 1.5% glutaraldehyde and 2.5% paraformaldehyde in 0.1M HCl-Na cacodylate buffer for 2 hours, then post-fixed for 90 minutes at 40°C with 1% osmium tetraoxide in the same buffer, and then incubated with 0.5% tannic acid for 30 minutes at room temperature. After dehydration in graded ethanol, and propylene oxide treatment, specimens were embedded in epoxy resin. Sections were cut with a diamond knife, stained with lead citrate and uranyl acetate and examined with a Hitachi H-7600 electron microscope.

Statistical analysis

Data are expressed as mean ± the standard error of the mean (s.e.m.). Statistical difference was analyzed with the Student's t test. A value of $P < 0.05$ was considered statistically significant.

Supplementary Material

Refer to Web version on PubMed Central for supplementary material.

Acknowledgments

We thank G. Michael Upchurch, Andrew Bachman, Eli Rhoades, and Jang Kim for technical assistance and other members of the Olson laboratory for valuable discussions and critical reading of the manuscript. We thank Dr. Linda Thompson (Oklahoma Medical Research Foundation) for discussion and reading of the manuscript. We also thank Dr. Jana Barlic-Dicen and Dr. Longbiao Yao (Oklahoma Medical Research Foundation) for help with atherosclerosis analysis, and Dr. Ming-Hui Zou (University of Oklahoma Health Sciences Center) for help with blood pressure measurements. We thank the OMRF COBRE Flow Cytometry Core for flow cytometry analysis; the OMRF COBRE Imaging Core facility for tissue processing; Dr. Weidong Wang for assistance with confocal microscopy; and Drs. David Brenner (UCSD), and Lothar Hennighausen (NIH/NIDDK) for sharing mouse strains. This study was supported by National Institutes of Health (NIH) grant P20-GM103636 (to L.E. Olson), P20-GM103441 (to L.E. Olson and F. Lupu), and DK087989 (to M. Hinsdale), and an Oklahoma Center for Adult Stem Cell Research (OCASCR) grant (to L.E. Olson). Dr. Lorin E. Olson is a Pew Scholar in Biomedical Research and this work was supported in part by the Pew Charitable Trusts.

References

1. Libby P, Ridker PM, Hansson GK. Progress and challenges in translating the biology of atherosclerosis. Nature. 2011; 473:317–325. [PubMed: 21593864]
2. Falk E. Pathogenesis of atherosclerosis. J Am Coll Cardiol. 2006; 47:C7–12. [PubMed: 16631513]
3. Bentzon JF, Otsuka F, Virmani R, Falk E. Mechanisms of plaque formation and rupture. Circ Res. 2014; 114:1852–1866. [PubMed: 24902970]
4. Virmani R, Kolodgie FD, Burke AP, Farb A, Schwartz SM. Lessons from sudden coronary death: a comprehensive morphological classification scheme for atherosclerotic lesions. Arterioscler Thromb Vasc Biol. 2000; 20:1262–1275. [PubMed: 10807742]
5. Schwartz SM, Galis ZS, Rosenfeld ME, Falk E. Plaque rupture in humans and mice. Arterioscler Thromb Vasc Biol. 2007; 27:705–713. [PubMed: 17332493]
6. Bentzon JF, Falk E. Atherosclerotic lesions in mouse and man: is it the same disease? Curr Opin Lipidol. 2010; 21:434–440. [PubMed: 20683327]
7. Newby AC, Zaltsman AB. Fibrous cap formation or destruction--the critical importance of vascular smooth muscle cell proliferation, migration and matrix formation. Cardiovasc Res. 1999; 41:345–360. [PubMed: 10341834]
8. Owens GK, Kumar MS, Wamhoff BR. Molecular regulation of vascular smooth muscle cell differentiation in development and disease. Physiol Rev. 2004; 84:767–801. [PubMed: 15269336]
9. Gomez D, Owens GK. Smooth muscle cell phenotypic switching in atherosclerosis. Cardiovasc Res. 2012; 95:156–164. [PubMed: 22406749]
10. Heldin CH, Westermark B, Wasteson A. Platelet-derived growth factor. Isolation by a large-scale procedure and analysis of subunit composition. Biochem J. 1981; 193:907–913. [PubMed: 7305965]
11. Ross R, Glomset J, Kariya B, Harker L. A platelet-dependent serum factor that stimulates the proliferation of arterial smooth muscle cells in vitro. Proc Natl Acad Sci U S A. 1974; 71:1207–1210. [PubMed: 4208546]
12. Corjay MH, Blank RS, Owens GK. Platelet-derived growth factor-induced destabilization of smooth muscle alpha-actin mRNA. J Cell Physiol. 1990; 145:391–397. [PubMed: 2273054]
13. Holycross BJ, Blank RS, Thompson MM, Peach MJ, Owens GK. Platelet-derived growth factor-BB-induced suppression of smooth muscle cell differentiation. Circ Res. 1992; 71:1525–1532. [PubMed: 1423945]
14. Andrae J, Gallini R, Betsholtz C. Role of platelet-derived growth factors in physiology and medicine. Genes Dev. 2008; 22:1276–1312. [PubMed: 18483217]
15. Raines EW. PDGF and cardiovascular disease. Cytokine Growth Factor Rev. 2004; 15:237–254. [PubMed: 15207815]
16. Kozaki K, et al. Blockade of platelet-derived growth factor or its receptors transiently delays but does not prevent fibrous cap formation in ApoE null mice. Am J Pathol. 2002; 161:1395–1407. [PubMed: 12368212]

17. Sano H, et al. Functional blockade of platelet-derived growth factor receptor-beta but not of receptor-alpha prevents vascular smooth muscle cell accumulation in fibrous cap lesions in apolipoprotein E-deficient mice. Circulation. 2001; 103:2955–2960. [PubMed: 11413086]
18. Olson LE, Soriano P. PDGFRbeta Signaling Regulates Mural Cell Plasticity and Inhibits Fat Development. Dev Cell. 2011; 20:815–826. [PubMed: 21664579]
19. Zernecke A, Shagdarsuren E, Weber C. Chemokines in atherosclerosis: an update. Arterioscler Thromb Vasc Biol. 2008; 28:1897–1908. [PubMed: 18566299]
20. Galkina E, et al. Lymphocyte recruitment into the aortic wall before and during development of atherosclerosis is partially L-selectin dependent. J Exp Med. 2006; 203:1273–1282. [PubMed: 16682495]
21. Galkina E, Ley K. Immune and inflammatory mechanisms of atherosclerosis (*). Annual review of immunology. 2009; 27:165–197.
22. Majesky MW, Dong XR, Hoglund V, Mahoney WM Jr, Daum G. The adventitia: a dynamic interface containing resident progenitor cells. Arterioscler Thromb Vasc Biol. 2011; 31:1530–1539. [PubMed: 21677296]
23. Basford JE, Moore ZW, Zhou L, Herz J, Hui DY. Smooth muscle LDL receptor-related protein-1 inactivation reduces vascular reactivity and promotes injury-induced neointima formation. Arterioscler Thromb Vasc Biol. 2009; 29:1772–1778. [PubMed: 19729608]
24. Boucher P, Gotthardt M, Li WP, Anderson RG, Herz J. LRP: role in vascular wall integrity and protection from atherosclerosis. Science. 2003; 300:329–332. [PubMed: 12690199]
25. Kolodgie FD, et al. Intraplaque hemorrhage and progression of coronary atheroma. N Engl J Med. 2003; 349:2316–2325. [PubMed: 14668457]
26. Michel JB, Virmani R, Arbustini E, Pasterkamp G. Intraplaque haemorrhages as the trigger of plaque vulnerability. European heart journal. 2011; 32:1977–1985. 1985a, 1985b, 1985c. [PubMed: 21398643]
27. Nakashima Y, Plump AS, Raines EW, Breslow JL, Ross R. ApoE-deficient mice develop lesions of all phases of atherosclerosis throughout the arterial tree. Arterioscler Thromb. 1994; 14:133–140. [PubMed: 8274468]
28. Reddick RL, Zhang SH, Maeda N. Atherosclerosis in mice lacking apo E. Evaluation of lesional development and progression. Arterioscler Thromb. 1994; 14:141–147. [PubMed: 8274470]
29. Rauch I, Muller M, Decker T. The regulation of inflammation by interferons and their STATs. Jak-Stat. 2013; 2:e23820. [PubMed: 24058799]
30. Vignais ML, Sadowski HB, Watling D, Rogers NC, Gilman M. Platelet-derived growth factor induces phosphorylation of multiple JAK family kinases and STAT proteins. Mol Cell Biol. 1996; 16:1759–1769. [PubMed: 8657151]
31. Choudhury GG, Ghosh-Choudhury N, Abboud HE. Association and direct activation of signal transducer and activator of transcription1alpha by platelet-derived growth factor receptor. J Clin Invest. 1998; 101:2751–2760. [PubMed: 9637709]
32. Klover PJ, et al. Loss of STAT1 from mouse mammary epithelium results in an increased Neu-induced tumor burden. Neoplasia. 2010; 12:899–905. [PubMed: 21076615]
33. Moulton KS, et al. Inhibition of plaque neovascularization reduces macrophage accumulation and progression of advanced atherosclerosis. Proc Natl Acad Sci U S A. 2003; 100:4736–4741. [PubMed: 12682294]
34. Vinchi F, et al. Atherogenesis and iron: from epidemiology to cellular level. Frontiers in pharmacology. 2014; 5:94. [PubMed: 24847266]
35. Fernandez-Hernando C, et al. Loss of Akt1 leads to severe atherosclerosis and occlusive coronary artery disease. Cell Metab. 2007; 6:446–457. [PubMed: 18054314]
36. Braun A, et al. Loss of SR-BI expression leads to the early onset of occlusive atherosclerotic coronary artery disease, spontaneous myocardial infarctions, severe cardiac dysfunction, and premature death in apolipoprotein E-deficient mice. Circ Res. 2002; 90:270–276. [PubMed: 11861414]
37. Lotzer K, et al. Mouse aorta smooth muscle cells differentiate into lymphoid tissue organizer-like cells on combined tumor necrosis factor receptor-1/lymphotoxin beta-receptor NF-kappaB signaling. Arterioscler Thromb Vasc Biol. 2010; 30:395–402. [PubMed: 20139367]

38. Krautler NJ, et al. Follicular dendritic cells emerge from ubiquitous perivascular precursors. Cell. 2012; 150:194–206. [PubMed: 22770220]
39. Grabner R, et al. Lymphotoxin beta receptor signaling promotes tertiary lymphoid organogenesis in the aorta adventitia of aged ApoE−/− mice. J Exp Med. 2009; 206:233–248. [PubMed: 19139167]
40. Boring L, Gosling J, Cleary M, Charo IF. Decreased lesion formation in CCR2−/− mice reveals a role for chemokines in the initiation of atherosclerosis. Nature. 1998; 394:894–897. [PubMed: 9732872]
41. Braunersreuther V, et al. Ccr5 but not Ccr1 deficiency reduces development of diet-induced atherosclerosis in mice. Arterioscler Thromb Vasc Biol. 2007; 27:373–379. [PubMed: 17138939]
42. Gu L, et al. Absence of monocyte chemoattractant protein-1 reduces atherosclerosis in low density lipoprotein receptor-deficient mice. Molecular cell. 1998; 2:275–281. [PubMed: 9734366]
43. Krohn R, et al. Y-box binding protein-1 controls CC chemokine ligand-5 (CCL5) expression in smooth muscle cells and contributes to neointima formation in atherosclerosis-prone mice. Circulation. 2007; 116:1812–1820. [PubMed: 17893273]
44. Heller EA, et al. Chemokine CXCL10 promotes atherogenesis by modulating the local balance of effector and regulatory T cells. Circulation. 2006; 113:2301–2312. [PubMed: 16682613]
45. Veillard NR, et al. Differential influence of chemokine receptors CCR2 and CXCR3 in development of atherosclerosis in vivo. Circulation. 2005; 112:870–878. [PubMed: 16061736]
46. Mach F, et al. Differential expression of three T lymphocyte-activating CXC chemokines by human atheroma-associated cells. J Clin Invest. 1999; 104:1041–1050. [PubMed: 10525042]
47. van Wanrooij EJ, et al. CXCR3 antagonist NBI-74330 attenuates atherosclerotic plaque formation in LDL receptor-deficient mice. Arterioscler Thromb Vasc Biol. 2008; 28:251–257. [PubMed: 18048768]
48. Ross R, Glomset JA. Atherosclerosis and the arterial smooth muscle cell: Proliferation of smooth muscle is a key event in the genesis of the lesions of atherosclerosis. Science. 1973; 180:1332–1339. [PubMed: 4350926]
49. Stary HC, et al. A definition of the intima of human arteries and of its atherosclerosis-prone regions. A report from the Committee on Vascular Lesions of the Council on Arteriosclerosis, American Heart Association. Arterioscler Thromb. 1992; 12:120–134. [PubMed: 1731855]
50. Ikari Y, McManus BM, Kenyon J, Schwartz SM. Neonatal intima formation in the human coronary artery. Arterioscler Thromb Vasc Biol. 1999; 19:2036–2040. [PubMed: 10479643]
51. Weninger WJ, Muller GB, Reiter C, Meng S, Rabl SU. Intimal hyperplasia of the infant parasellar carotid artery: a potential developmental factor in atherosclerosis and SIDS. Circ Res. 1999; 85:970–975. [PubMed: 10559145]
52. Rong JX, Shapiro M, Trogan E, Fisher EA. Transdifferentiation of mouse aortic smooth muscle cells to a macrophage-like state after cholesterol loading. Proc Natl Acad Sci U S A. 2003; 100:13531–13536. [PubMed: 14581613]
53. Feil S, et al. Transdifferentiation of vascular smooth muscle cells to macrophage-like cells during atherogenesis. Circ Res. 2014; 115:662–667. [PubMed: 25070003]
54. Tabas I, Williams KJ, Boren J. Subendothelial lipoprotein retention as the initiating process in atherosclerosis: update and therapeutic implications. Circulation. 2007; 116:1832–1844. [PubMed: 17938300]
55. Cuff CA, et al. The adhesion receptor CD44 promotes atherosclerosis by mediating inflammatory cell recruitment and vascular cell activation. J Clin Invest. 2001; 108:1031–1040. [PubMed: 11581304]
56. Doran AC, Meller N, McNamara CA. Role of smooth muscle cells in the initiation and early progression of atherosclerosis. Arterioscler Thromb Vasc Biol. 2008; 28:812–819. [PubMed: 18276911]
57. Silvennoinen O, Schindler C, Schlessinger J, Levy DE. Ras-independent growth factor signaling by transcription factor tyrosine phosphorylation. Science. 1993; 261:1736–1739. [PubMed: 8378775]

58. Durbin JE, Hackenmiller R, Simon MC, Levy DE. Targeted disruption of the mouse Stat1 gene results in compromised innate immunity to viral disease. Cell. 1996; 84:443–450. [PubMed: 8608598]

59. Meraz MA, et al. Targeted disruption of the Stat1 gene in mice reveals unexpected physiologic specificity in the JAK-STAT signaling pathway. Cell. 1996; 84:431–442. [PubMed: 8608597]

60. Marra F, Choudhury GG, Abboud HE. Interferon-gamma-mediated activation of STAT1alpha regulates growth factor-induced mitogenesis. J Clin Invest. 1996; 98:1218–1230. [PubMed: 8787685]

61. Ramana CV, et al. Stat1-independent regulation of gene expression in response to IFN-gamma. Proc Natl Acad Sci U S A. 2001; 98:6674–6679. [PubMed: 11390994]

62. Tellides G, et al. Interferon-gamma elicits arteriosclerosis in the absence of leukocytes. Nature. 2000; 403:207–211. [PubMed: 10646607]

63. Yamamoto H, Crow M, Cheng L, Lakatta E, Kinsella J. PDGF receptor-to-nucleus signaling of p91 (STAT1 alpha) transcription factor in rat smooth muscle cells. Exp Cell Res. 1996; 222:125–130. [PubMed: 8549654]

64. Magness ST, Bataller R, Yang L, Brenner DA. A dual reporter gene transgenic mouse demonstrates heterogeneity in hepatic fibrogenic cell populations. Hepatology. 2004; 40:1151–1159. [PubMed: 15389867]

65. Song P, et al. AMPKalpha2 deletion exacerbates neointima formation by upregulating Skp2 in vascular smooth muscle cells. Circ Res. 2011; 109:1230–1239. [PubMed: 21980125]

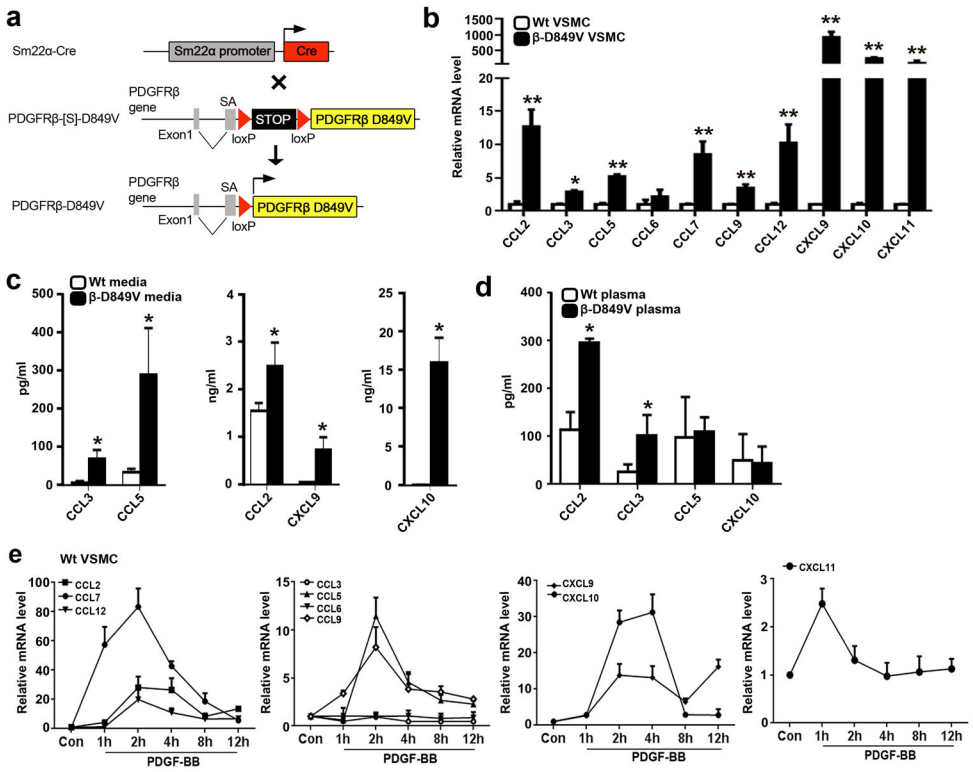

Figure 1. PDGF signaling induces VSMCs to release chemokines

(a) Strategy for activating a conditional *PDGFRβ*^{D849V} allele in VSMCs. The conditional *PDGFRβ*^{D849V} allele consists of a loxP-flanked stop cassette preceding a full-length mouse PDGFRβ cDNA with a single amino acid substitution (D849V), which was targeted to the *Pdgfrβ* gene. When the conditional allele is present in Sm22α-Cre transgenic mice, the stop is removed in VSMCs and PDGFRβ^{D849V} is expressed. SA = splice acceptor. (b) Fold change in chemokine mRNA levels in cultured VSMCs from *PDGFRβ*^{Sm22D849V} (β-D849V) mutant mice and Sm22α-Cre (Wt) control mice was determined by quantitative RT-PCR. Results are shown as fold increase in mutant over control, n=3 different VSMC isolates per genotype. (c) Quantification of chemokines secreted into the media of cultured VSMCs as determined by ELISA, n=3 different VSMC isolates per genotype. (d) Quantification of chemokines in plasma from mutant mice and control mice as determined by ELISA, n=3 mice per genotype. (e) Fold change in chemokine mRNA levels in cultured Wt VSMCs treated with 10ng ml^{-1} PDGF-BB ligand for the indicated times was determined by quantitative RT-PCR. Results are shown as fold increase in treated cells over untreated controls, n=3 different VSMC isolates. All data were assessed using Student's *t*-test and are present as mean ± s.e.m. **P*<0.05; ***P*<0.01.

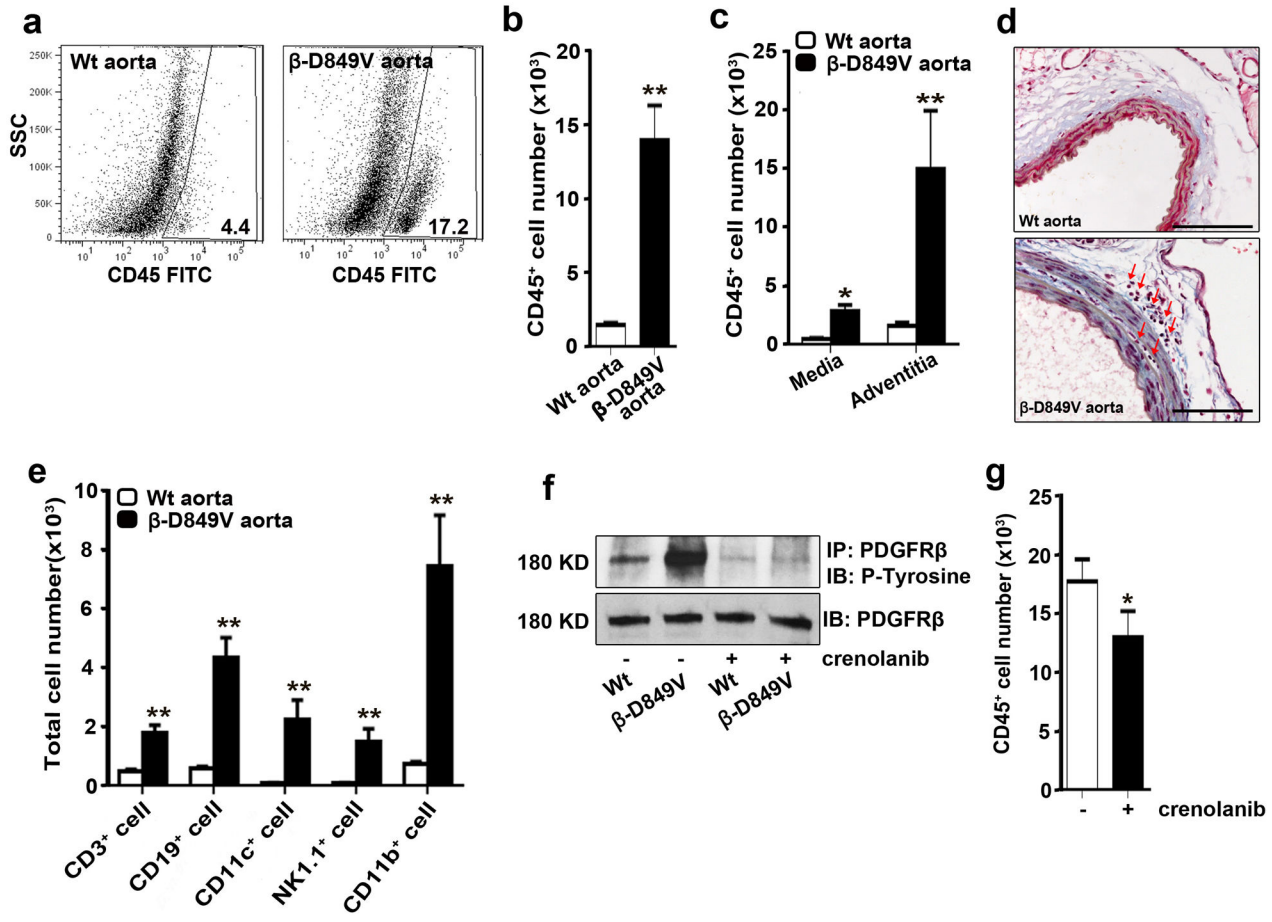

Figure 2. PDGF signaling in VSMCs causes inflammation of the aorta

(a) Flow cytometric analysis of cells in the aorta of *PDGFRβ*^{Sm22D849V} (β-D849V) mutant mice and Sm22α-Cre (Wt) control mice after enzymatic digestion. Numerical data indicate the percentage of CD45^{+} leukocytes among the total cells analyzed. Representative plots from three aortas of each genotype are shown. (b, c) Quantification of CD45^{+} leukocytes in the whole aorta or the separated media and adventitia as measured by flow cytometry, n=3 mice per genotype for each type of analysis. (d) Distribution of leukocytes (red arrows) in the media and adventitia was determined by staining cross sections of the thoracic aorta with Masson's trichrome. Representative sections from 3 aortas of each genotype are shown. Scale bar, 100μm (e) Quantification of immune cell types in the aortic wall as measured by flow cytometry using fluorescent-conjugated antibodies: APC-CD3; APC.Cy7-CD19; PE-CD11c; PE.Cy7-NK1.1; PerCy5.5-Mac1, n=3 mice per genotype. (f) Phosphorylation of immunoprecipitated PDGFRβ from cultured VSMCs was determined by Western blotting with anti-phosphotyrosine antibody. PDGFRβ-D849V tyrosine kinase activity was inhibited by treatment with the PDGFR inhibitor Crenolanib (400ng ml^{-1}) for 2 hours prior to cell lysis. Representative blot from 2 experiments is shown. (g) Quantification of CD45^{+} leukocytes in the whole aorta of *PDGFRβ*^{Sm22D849V} mutant mice was measured by flow cytometry. Injecting mice with 15mg kg^{-1} Crenolanib for 5 consecutive days before sacrifice led to attenuation of CD45^{+} leukocytes in the aortic wall, n=3 mice per treatment.

All data were assessed using Student's *t*-test and are present as mean ± s.e.m. **P*<0.05; ***P*<0.01.

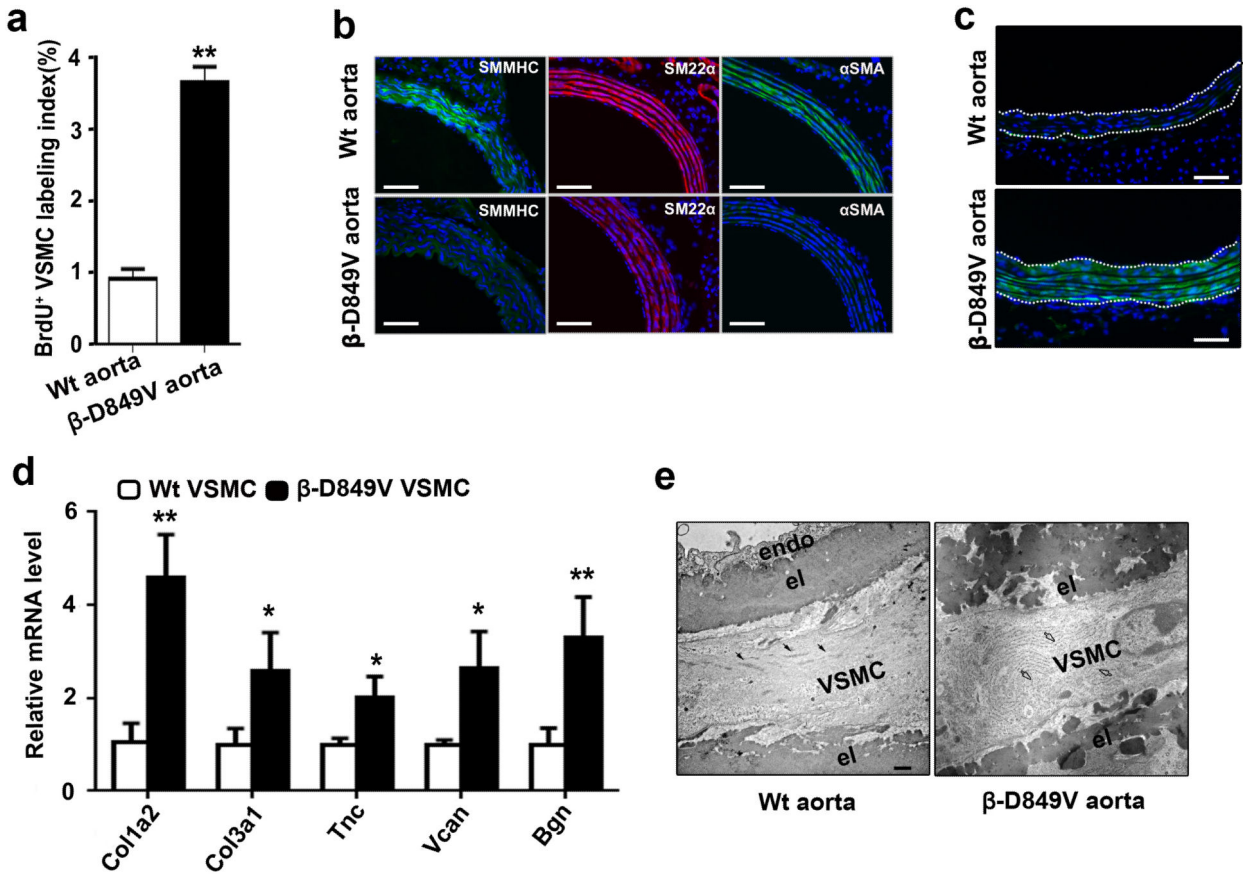

Figure 3. *PDGFRβ*^{Sm22D849V} mutant mice have constitutively dedifferentiated VSMCs

(a) Proliferation of VSMCs in the thoracic aorta of 4-week old *PDGFRβ*^{Sm22D849V} (β-D849V) mutant or Sm22α-Cre (Wt) control mice was measured by immunohistochemical detection of BrdU incorporation. Data represent the percentage of VSMCs that were BrdU^{+}, n=3 aortas per genotype. (b) Mature VSMC marker expression in the cross-sectioned thoracic aorta of 4-week old mice was determined by immunofluorescence, with DAPI as a nuclear counterstain. Representative images from three aortas of each genotype are shown. Scale bar, 50μm. (c) Expression of a Collagen1a1-EGFP transgenic reporter in mutant or control mice was determined by epifluorescence with DAPI as a nuclear counterstain. The media is outlined. Representative images from three aortas of each genotype are shown. Scale bar, 50μm. (d) Fold change in extracellular matrix protein mRNA levels in cultured VSMCs from mutant and control mice was determined by quantitative RT-PCR. Results are shown as fold increase in mutant over control, n=4 cell isolates per genotype. (e) VSMC ultrastructure in the thoracic aorta of 2-week old mutant or control mice was determined by transmission electron microscopy. Black arrows identify VSMC contractile bundles in the control; open arrows identify rough endoplasmic reticulum in the mutant; endo = endothelium; el = elastic lamellae. Scale bar, 50nm. All data were assessed using Student's *t*-test and are present as mean ± s.e.m. **P*<0.05; ***P*<0.01.

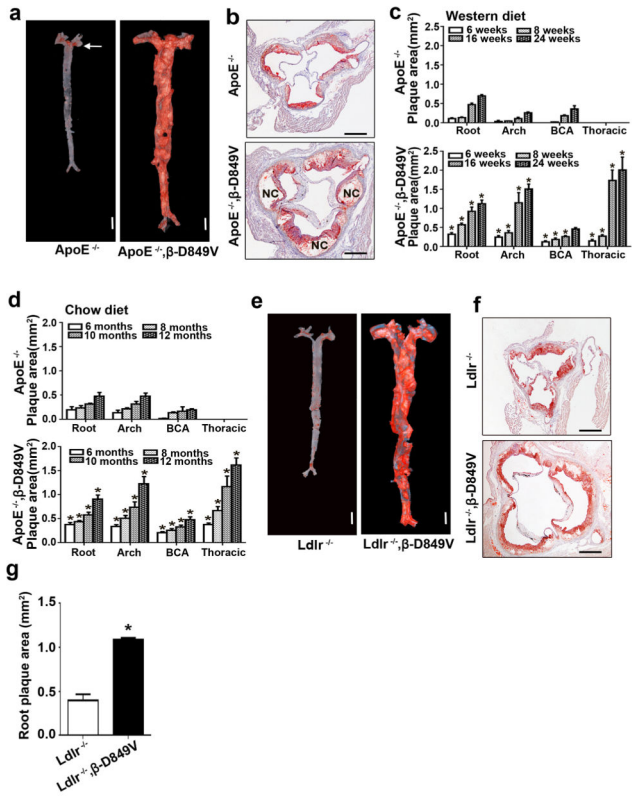

Figure 4. PDGF signaling amplifies atherosclerosis in hypercholesterolemic mice

(a) Distribution of atherosclerotic plaques on the aortic lumen of *ApoE,PDGFRβ*^{Sm22D849V} (ApoE$^{-/-}$,β-D849V) mutants and *ApoE*$^{-/-}$ controls after 16 weeks of WD was determined by *en face* Oil red O staining. Representative pictures of three aortas of each genotype are shown. Arrow indicates aortic arch plaques in the *ApoE* control. Scale bar, 5mm. (b) Distribution of plaques in the aortic root after 16 weeks of WD was determined by staining sections with Oil red O. Representative pictures of three roots of each genotype are shown. NC = necrotic core. Scale bar, 500μm. (c, d) Quantification of plaque cross-sectional area at the aortic root, aortic arch, brachiocephalic artery (BCA), and thoracic aorta in mice fed WD (c) or chow diet (d) for the indicated times, n=10 mice of each genotype per time point; **P*<0.01 by Student's *t*-test for comparison between mutant and control at each time point. (e) Distribution of atherosclerotic plaques on the aortic lumen of *Ldlr,PDGFRβ*^{Sm22D849V} (Ldlr$^{-/-}$,β-D849V) mutants and *Ldlr*$^{-/-}$ controls after 16 weeks of WD was determined by *en face* Oil red O staining. Representative pictures of three aortas of each genotype are shown. Scale bar, 5mm. (f) Distribution of plaques in the aortic root after 16 weeks of WD was determined by staining sections with Oil red O. Representative pictures of six roots of each genotype are shown. Scale bar, 500μm. (g) Quantification of plaque cross-sectional area in the aortic root, n=6 roots of each genotype; **P*<0.01 by Student's *t*-test. All data represent mean ± s.e.m.

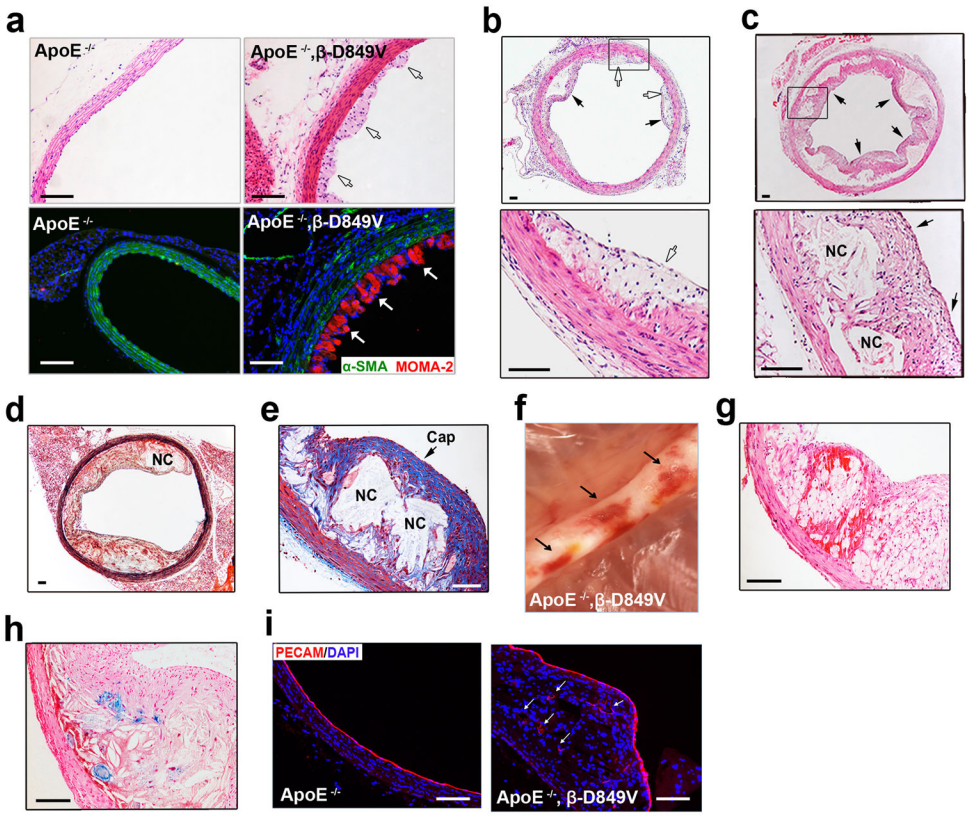

Figure 5. Plaque initiation, progression to fibroatheroma and intraplaque hemorrhage

(a) Plaque initiation in the thoracic aorta of *ApoE,PDGFRβ*^{Sm22D849V} (ApoE$^{-/-}$,β-D849V) mutant and *ApoE*$^{-/-}$ control mice after 6 weeks of WD was assessed by staining cross sections of the aorta with hematoxylin and eosin (top panels) or with fluorescent antibodies to identify VSMCs (αSMA, green) and macrophage foam cells (MOMA-2, red). Representative pictures of three aortas of each genotype are shown. Only the mutant has subendothelial foam cell plaques in the thoracic aorta (white arrows). Scale bar, 100μm. (b, c) Histological analysis of plaque progression in the thoracic aorta of *ApoE,PDGFRβ*^{Sm22D849V} mice after 8 weeks (b) or 24 weeks (c) of WD. Shown are low magnification pictures (top), and high magnification pictures of the boxed areas (bottom), which are representative of at least six mutant aortas analyzed per time point. White arrows indicate foam cells, black arrows indicate fibrous caps, NC = necrotic core. Scale bar, 100μm. (d, e) Histological analysis of advanced plaques in *ApoE,PDGFRβ*^{Sm22D849V} mice after 16 or 24 weeks of WD. Sections were stained with (d) Movat's pentachrome (16 weeks WD) or (e) Masson's trichrome (24 weeks WD). Scale bar, 125μm. (f) Digital photograph of three sites of hemorrhage (arrows) in the *ApoE,PDGFRβ*^{Sm22D849V} thoracic aorta *in situ* after 16 weeks of WD. Before photography, the mouse was perfused through the heart and the aorta was cleared of adipose tissue. (g, h) Histological analysis of intraplaque ruptures was performed with (g) hematoxylin and eosin or (h) Prussian blue and nuclear fast red to demonstrate intraplaque hemorrhage with no evidence of fibrous cap rupture. Scale bar, 100μm. (i) Immunofluorescent analysis of endothelial cells in mutant and *ApoE* control

thoracic aortas after 16 weeks of WD. Representative images of PECAM staining are shown. Arrows indicate neovessels in the mutant plaque. Scale bar, 100μm.

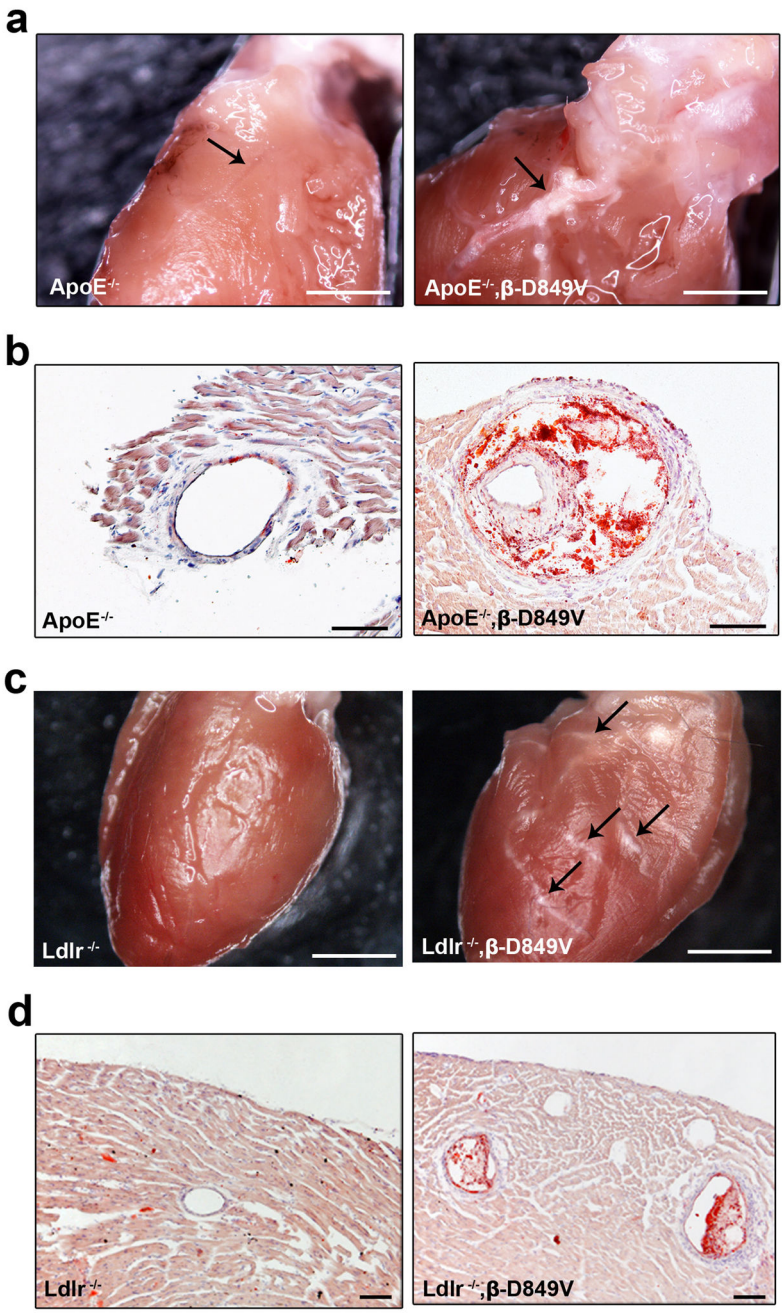

Figure 6. Coronary atherosclerosis

(a) Coronary artery plaques appear in *ApoE,PDGFRβ*^{Sm22D849V} mice after 10 months of chow diet but not *ApoE* control mice. Arrow indicates the left coronary artery. Pictures are representative of coronary plaques in 7 out of 10 mutants after >10 months of chow diet. (b) Cross sections through the left coronary artery were stained with Oil red O and hematoxylin. Scale bar, 100μm. (c) Coronary artery plaques in *Ldlr,PDGFRβ*^{Sm22D849V} mice after 16 weeks of WD, but not *Ldlr* control mice. Arrows identify plaques in multiple arteries on the left anterior surface of the heart. Pictures are representative of plaques in 5 out of 7 mutants

after >16 weeks of WD. (d) Cross sections through the heart were stained with Oil red O and hematoxylin. Scale bars, 1mm (a), 200μm (b, d), 2mm (c).

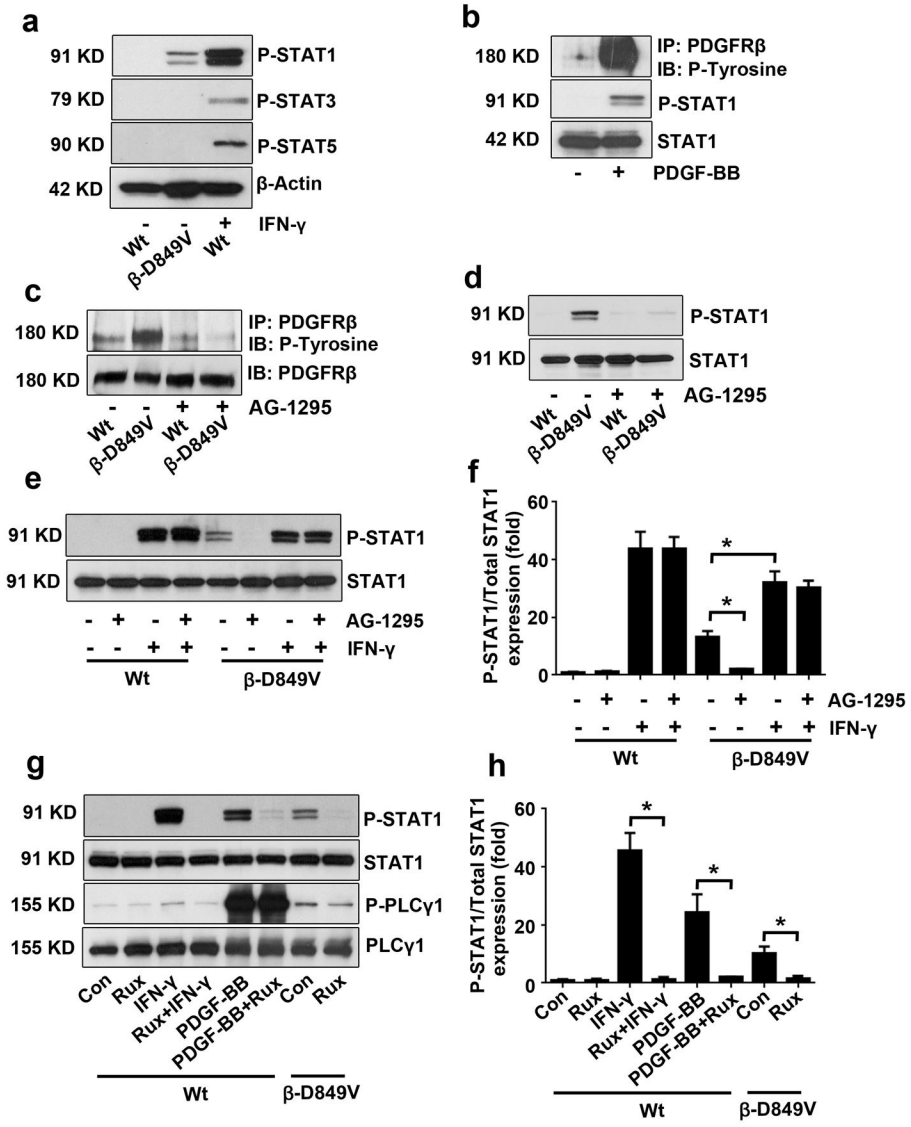

Figure 7. PDGF signaling activates STAT1 in VSMCs

(a) Tyrosine phosphorylation of STAT1, STAT3, and STAT5 in cultured VSMCs from *PDGFRβ*^{Sm22D849V} (β-D849V) mutant and Sm22α-Cre (Wt) control mice was determined by Western blot. As a positive control, VSMCs were treated with 10ng ml^{-1} mouse IFN-γ for 30 min. (b) Phosphorylation of PDGFRβ and STAT1 in control VSMCs after serum starvation and treatment with 10 ng ml^{-1} PDGF-BB for 15 minutes was determined by Western blot. PDGFRβ was immunoprecipitated from cell lysate and then phosphorylation was detected with anti-phosphotyrosine antibody. Phospho-STAT1 was detected in cell lysate with p-Y701 antibody. (c, d) PDGFRβ and STAT1 phosphorylation in *PDGFRβ*^{Sm22D849V} mutant and control VSMCs were analyzed by Western blotting after 16 hrs treatment with the PDGFR inhibitor 10 μM AG-1295. (e) STAT1 phosphorylation in *PDGFRβ*^{Sm22D849V} mutant and control VSMCs were analyzed by Western blotting after 16 hrs treatment with 10 μM AG-1295 followed by vehicle or 10ng ml^{-1} mouse IFN-γ for 30 min. (f) Quantification of Western blots in (e) by densitometry shown as fold change over

untreated Wt (lane 1). (g) STAT1 and PLCγ1 phosphorylation in *PDGFRβ*^{Sm22D849V} mutant and control VSMCs were analyzed by Western blotting after 16 hrs treatment with the JAK1/JAK2 inhibitor Ruxolitinib (10 μM) followed by 10ng ml^{-1} mouse IFN-γ for 30 minutes or 10 ng ml^{-1} PDGF-BB for 10 minutes. (h) Quantification of Western blots in (g) by densitometry shown as fold change over untreated Wt (lane 1). All data represent mean ± s.e.m. All experiments were performed at least three times; *P<0.01 by Student's t-test

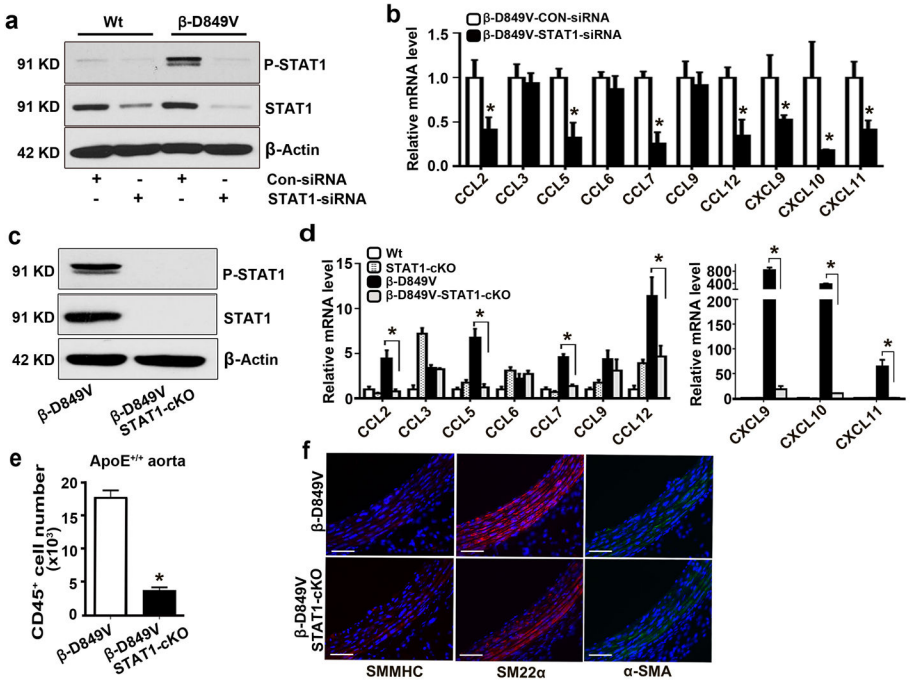

Figure 8. STAT1 regulates chemokines and inflammation in *PDGFRβ*^{Sm22D849V} mice

(a) Expression of total STAT1 and STAT1 p-Y701 in *PDGFRβ*^{Sm22D849V} (β-D849V) mutant and Sm22α-Cre (Wt) control VSMCs after transfection with control or STAT1-blocking siRNA was analyzed by Western blotting. (b) Fold change in chemokine mRNA levels in cultured VSMCs from mutant mice was determined by quantitative RT-PCR. Results are shown as fold change in STAT1 siRNA compared to control siRNA, n=4 transfections per siRNA. (c) Expression of total STAT1 and p-Y701 STAT1 in *PDGFRβ*^{Sm22D849V} (β-D849V) single mutant and *STAT1*^{Sm22CKO}*PDGFRβ*^{Sm22D849V} (β-D849V,STAT1-cKO) double mutant VSMCs was analyzed by Western blotting. (d) Fold change in chemokine mRNA levels in Wt, *STAT1*^{Sm22CKO} (STAT1-cKO), *PDGFRβ*^{Sm22D849V} (β-D849V) single mutant, and *STAT1*^{Sm22CKO}*PDGFRβ*^{Sm22D849V} (β-D849V,STAT1-cKO) double mutant VSMCs was determined by quantitative RT-PCR. Results are shown as fold change compared to Wt, n=3 different VSMC isolates per genotype. (e) Quantification of CD45^{+} leukocytes in the whole aorta of single mutant and double mutant mice (all *ApoE*$^{+/+}$) as measured by flow cytometry, n=3 mice per genotype. (f) Mature VSMC marker expression in the cross-sectioned thoracic aorta of 8-week old mice was determined by immunofluorescence, with DAPI as a nuclear counterstain. Representative images from three aortas of each genotype are shown. Scale bar, 50μm. All data were assessed using Student's *t*-test and are present as mean ± s.e.m. **P*<0.01.

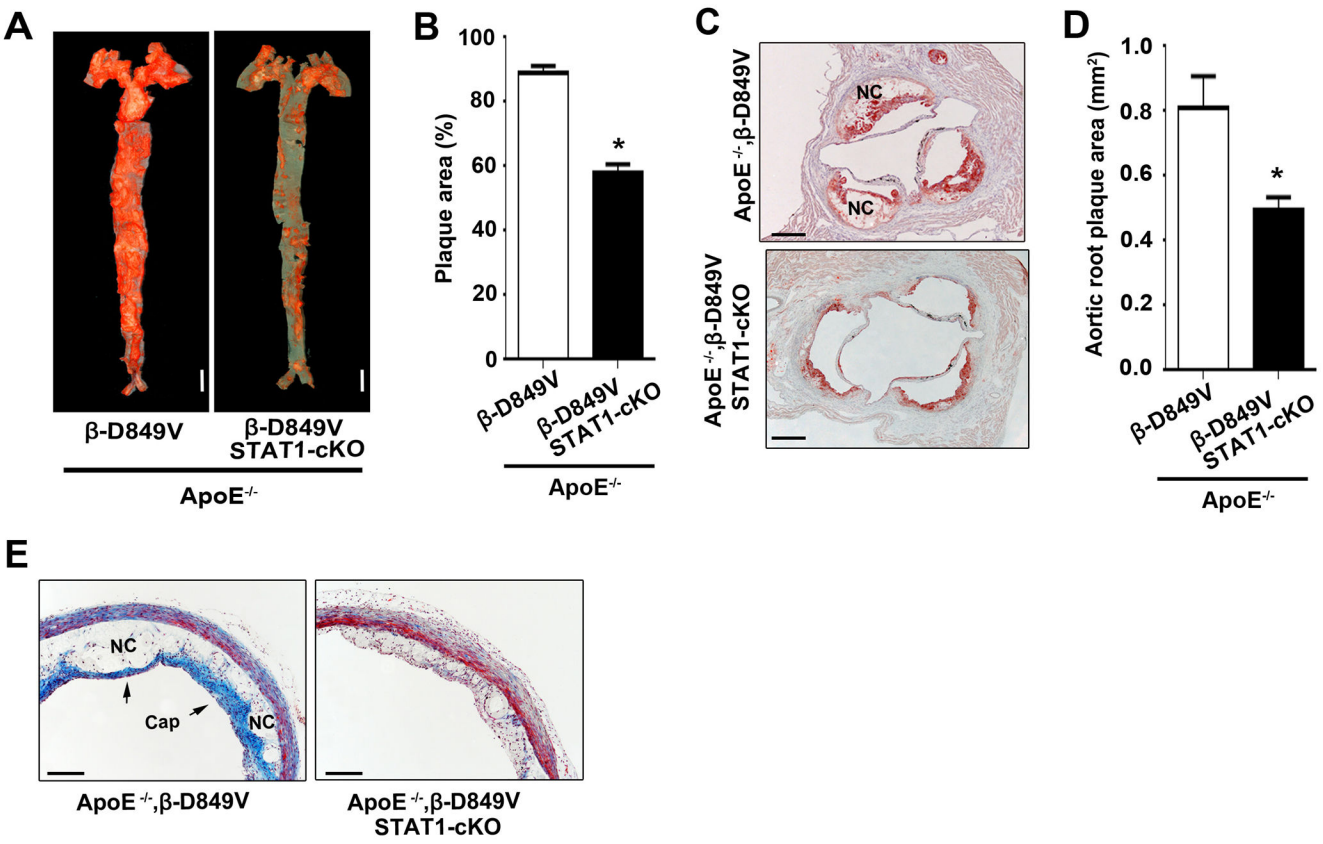

Figure 9. PDGF/STAT1-regulated inflammation amplifies atherosclerosis

(a) Distribution of atherosclerotic plaques on the aortic lumen of *ApoE,PDGFRβ*^{Sm22D849V} mutants and *ApoE,STAT1*^{Sm22CKO}*PDGFRβ*^{Sm22D849V} double mutants after 12 weeks of WD was determined by *en face* Oil red O staining. Representative pictures of six aortas of each genotype are shown. Scale bar, 5mm. (b) Quantification of plaque area as a percentage of total surface area of the aorta, n=6 aortas per genotype. (c) Distribution of plaques in the aortic root after 12 weeks of WD was determined by staining sections with Oil red O. Representative pictures of six roots of each genotype are shown. NC = necrotic core. Scale bar, 500μm. (d) Quantification of plaque cross-sectional area in the aortic root, n=6 roots per genotype. (e) Histological analysis of plaque morphology in the thoracic aorta after 12 weeks of WD was determined by trichrome staining. Scale bar, 250μm. Representative pictures of three aortas of each genotype are shown. All data represent mean ± s.e.m. **P*<0.01 by Student's *t*-test.

Table I

Serum lipid profiles.

Group	Diet	Cholesterol (mg/dl)	Triglyceride (mg/dl)
Wild type	Chow	97.4 ± 26.9	75.3 ± 12.2
β-D849V	Chow	91.2 ± 15.9	64.8 ± 19.2
Wild type	WD	156.1 ± 35.9	100.8 ± 13.6
β-D849V	WD	143.5 ± 23.4	114.5 ± 17.6
$ApoE^{-/-}$	Chow	523.6 ± 80.1	126.3 ± 15.2
$ApoE^{-/-}$, β-D849V	Chow	581.3 ± 56.2	134.8 ± 18.7
$ApoE^{- -}$	WD	1771.0 ± 204.3	130.8 ±13.6
$ApoE^{-/-}$, β-D849V	WD	1974.0 ± 178.2	124.5 ±25.4

Data represent mean ± s.e.m.; n = 5 mice for each group.